

# Morphological changes towards enhancing piezoelectric properties of PVDF electrical generators using cellulose nanocrystals

Hossein Fashandi · Mohammad Mahdi Abolhasani · Parastoo Sandoghdar · Nima Zohdi · Quanxiang Li · Mino Naebe

Received: 3 June 2016 / Accepted: 7 September 2016 / Published online: 15 September 2016  
© Springer Science+Business Media Dordrecht 2016

**Abstract** For the first time, a nanocomposite of poly(vinylidene fluoride)/cellulose nanocrystal (PVDF/CNC) is developed as a piezoelectric energy harvester. This is implemented through electrospinning of PVDF solutions containing different levels of CNC loading, i.e., 0, 1, 3 and 5 % with respect to PVDF weight. Analytical techniques including DSC, FTIR and WAXD are conducted to monitor the polymorphism evolution within electrospun nanocomposites as the CNC content is varied. The results imply that CNCs at the optimum concentration (3 and 5 %) can effectively nucleate  $\beta$  crystalline phases. The nucleation of  $\alpha$  crystalline phases is also prevented when CNCs are present within the structure of PVDF electrospun fibers. These changes in polymorphism give PVDF/CNC nanocomposites

enhanced piezoelectric characteristics compared to pure PVDF nanofibers. We have demonstrated that the developed nanocomposites can charge a 33- $\mu$ F capacitor over 6 V and light up a commercial LED for more than 30 s. It is envisaged that the PVDF/CNC nanocomposites provide the opportunity for the development of efficient electrical generators as self-powering devices to charge portable electronics.

**Keywords** PVDF · Cellulose nanocrystal · Electrospinning · Nanocomposite · Electrical power generator · Energy harvesting · Piezoelectricity

---

**Electronic supplementary material** The online version of this article (doi:[10.1007/s10570-016-1070-3](https://doi.org/10.1007/s10570-016-1070-3)) contains supplementary material, which is available to authorized users.

---

H. Fashandi (✉) · P. Sandoghdar  
Department of Textile Engineering, Isfahan University of Technology, Isfahan 84156-83111, Iran  
e-mail: h.fashandi@cc.iut.ac.ir

M. M. Abolhasani (✉)  
Chemical Engineering Department, University of Kashan, Kashan, Iran  
e-mail: abolhasani@kashanu.ac.ir

N. Zohdi · Q. Li · M. Naebe  
Institute for Frontier Materials, Deakin University, Waurn Ponds, VIC 3216, Australia

## Introduction

Nowadays, the energy supply for electrical devices with low-energy consumption as well as portable electronics has been widely acknowledged. In this regard, energy scavenging from the our surrounding sources (e.g., sound, mechanical vibrations, thermal energy, solar energy, wind, water waves, etc.) has received great interest as a promising power source to supply energy as well as being a potential alternative to the conventional rechargeable batteries (Lee et al. 2012; Soin et al. 2014; Pu et al. 2015; Xie et al. 2013; Zhu et al. 2014; Xie et al. 2014; Chang et al. 2010, 2012).

Energy scavenging from the environment is primarily conducted based on piezoelectric, thermoelectric and photovoltaic phenomena; among these, a great

deal of attention has been devoted to converting mechanical strains because of bending, vibration, stretching or compression into electricity to make wireless self-powered systems (Chang et al. 2010). Furthermore, piezoelectric generators have been produced in a variety of structures including:

- *polymer film* prepared from poly(vinylidene fluoride) (PVDF) in flat and rolled form (Sun et al. 2010; Seminara et al. 2011; El Achaby et al. 2012; Mao et al. 2014; Chen and Zhang 2015; Cha et al. 2011; Yee et al. 2007; Pörhönen et al. 2014);
- *nanowire and nanorods* made of inorganic materials such as ZnO (Cha et al. 2010; Wang and Song 2006), 1-D ZnO nanorods on a 2D graphene electrode (Choi et al. 2010), CdS (Lin et al. 2008), GaN (Wang et al. 2010) and ZnS (Lu et al. 2009);
- *a hybrid piezoelectric structure* made of ZnO nanowires in a matrix of PVDF (Lee et al. 2012);
- *three-dimensional spacer fabric* knitted from piezoelectric PVDF monofilaments (Soin et al. 2014);
- *PVDF melt-spun microfibers* (Hadimani et al. 2013);
- *poly(vinylidene-co-trifluoroethylene) [P(VDF-TrFE)] nanofibrous yarn* (Baniasadi et al. 2015);
- *nanofibers* electrospun from solutions composed of PZT ceramic (Chang et al. 2012; Chen et al. 2010; Shiyu et al. 2006); PVDF polymer (Chang et al. 2010, 2012; Gheibi et al. 2014; Ding et al. 2015; Zeng et al. 2013); P(VDF-TrFE) copolymer (Baniasadi et al. 2016; Persano et al. 2013; Mandal et al. 2011).

The literature survey shows that piezoelectric energy scavengers have been manufactured using both polymeric and inorganic materials as well as a combination of those. Although the inorganic materials have been used in energy harvesting fairly successfully, there are some disadvantages associated with their application that hinder their true potentials. This includes the high cost as well as not being easily integratable and scalable. Additionally, they fail at very low strains, i.e., above 1 %. However, polymer-based piezoelectric electrical power generators exhibit excellent flexibility and enjoy a lower weight (Soin et al. 2014; Zeng et al. 2013; Lee et al. 2013).

Among different polymeric piezoelectric-based energy-scavenging structures, nanofibers are known

as robust energy generators. This lies mainly in the fact that the high electrical field and stretching during electrospinning eliminate any requirements for post-treatment processes including electric poling and mechanical stretching. This is because post-treatment processes are vital to form and promote piezoelectric polymorph formation in PVDF films and microfibers. Furthermore, it has been demonstrated that under cyclic impact, piezoelectric PVDF nanofiber generators can potentially outperform PVDF films (Chang et al. 2010; Yee et al. 2007; Zeng et al. 2013). Therefore, priority is given to polymeric nanofibers for making highly efficient electrical power generators.

PVDF is a thermoplastic polymer that is crystallized in five different polymorphs including  $\alpha$ ,  $\beta$ ,  $\gamma$ ,  $\delta$  and  $\epsilon$ , of which the  $\beta$  phase is responsible for the piezoelectric properties. It is also well known that piezoelectricity is highly dependent on the orientation of dipoles in the  $\beta$  phase (Chang et al. 2012; Mao et al. 2014; Chen and Zhang 2015; Hadimani et al. 2013; Baqeri et al. 2015; Abolhasani 2015; Abolhasani et al. 2014a, 2015a, b, c, 2016; Martins et al. 2014). In this respect, enormous efforts have been made to further enhance the energy conversion efficiency of piezoelectric nanofibers focusing on increasing the  $\beta$  phase content and the orientation of molecular dipoles. Some of the approaches include use of modified electrospinning techniques such as near- and far-field electrospinning of PVDF and P(VDF-TrFE) nanofibers, electrospinning of PVDF nanofibers using modified collectors as well as various inclusions of nanomaterials, e.g., nanoclay, MWCNT and NaNbO<sub>3</sub>, into PVDF-based solutions prior to electrospinning (Chang et al. 2010; Ding et al. 2015; Zeng et al. 2013; Mandal et al. 2011; Pu et al. 2010; Yee et al. 2008; Liu et al. 2010, 2013; Yu and Cebe 2009; Ahn et al. 2013).

As reported, these procedures could significantly improve the piezoelectric properties of PVDF. In spite of the numerous efforts made in the field of PVDF electrospun nanocomposites (Zeng et al. 2013; Liu et al. 2010, 2013; Yu and Cebe 2009; Ahn et al. 2013), there are still opportunities to further improve the piezoelectric performance of PVDF-based nanofibers. Recently, nanocomposite films of PVDF and cellulose nanocrystals (CNCs) were prepared through solution casting by Zhang et al. (2015). It was demonstrated that CNCs can remarkably improve several PVDF properties including the hydrophilicity, thermal stability and

crystallinity. The nucleating role of CNCs in the crystallization of PVDF was also discussed.

CNCs with whisker-like shape have high tensile strength and an elastic modulus estimated as high as 250 GPa (Zimmermann et al. 2004). Additionally, CNCs exhibit a group of superior properties including biocompatibility, existence in abundance and biodegradability.

Besides PVDF, CNC has also made inroads into making nanocomposites with excellent properties using other polymers such as polyvinyl alcohol (Peresin et al. 2010), poly ethylene oxide (Zhou et al. 2011), poly(lactic acid) (Shi et al. 2012), poly(vinylidene fluoride-co-hexafluoro propylene) (PVDF-HFP) (Lalia et al. 2012), polystyrene (PS) (Huan et al. 2015) and even a nonpolymeric matrix, e.g., cement paste (Cao et al. 2015).

Despite the outstanding and exclusive features of CNCs along with their nucleating roles for PVDF, there is no report on the preparation of PVDF/CNC for the purpose of electrical power generators. The present work aims to produce PVDF/CNC generators through electrospinning and to investigate whether CNCs can promote the piezoelectric properties of PVDF nanofibers. The possible influence of CNC's impact on PVDF nanofiber morphology is also discussed through a variety of analytical techniques.

## Experimental

### Materials

Poly(vinylidene fluoride) (PVDF) (Kynar<sup>®</sup> 761A Powder,  $M_w = 495,000$  g/mol, MFI: 2.0–6.0 g/10 min (ASTM D1238, 230 °C, 12.5 kg) was purchased from Arkema<sup>®</sup> Inc. Dimethylformamide (DMF) and sulfuric acid were supplied by Sigma Aldrich, Inc. Cotton linters were supplied by Linter Pak Co., Behshahr, Iran.

### Preparation of cellulose nanocrystals (CNCs)

Controlled acid hydrolysis of cotton linters was used as a fairly simple technique to prepare CNCs. This technique works based on the higher resistance of crystalline regions to acid attacks than disordered and partially crystalline regions of cellulose (Habibi et al. 2010). Cotton linters were first vacuum oven dried at

40 °C for 24 h. The dried samples were kept in a desiccator to avoid water absorption. Samples were hydrolyzed using sulfuric acid (65 wt%) for 30 min. The temperature was kept constant at 40 °C throughout the hydrolysis process. The linter-to-acid ratio was chosen to be 1:10, i.e., 10 ml acid:1 g linter. To stop the reaction, tenfold distilled water was added to the hydrolysis vessel for several times until reaching neutral pH while the sample container was kept in an ice bath. Then, the hydrolyzed samples were centrifuged at 6000 rpm for 20 min, and the redundant solution was removed. As the last stage, to remove the residual sulfuric acid, hydrolyzed samples were dialyzed against deionized water for 1 week using a membrane with MWCO of 12,000.

### Characterization of PVDF/DMF solutions with different CNC contents

The shear viscosity of PVDF/DMF solutions with different CNC contents as a function of the shear rate was measured using a Rotovisco RV12 viscometer (Haake, Germany) at temperature controlled at 25 °C ( $\pm 2$  °C).

The electrical conductivity and surface tension of PVDF/DMF solutions with different CNC loadings were also measured using a JENWAY 3540 pH/conductivity meter (designed and manufactured in the EU by Barloworld Scientific, Ltd.) and DCAT 11 (Data-physics, Germany), respectively. For each mixture, the value averaged over at least five measurements was reported.

### Electrospinning of PVDF/CNC nanocomposites

For electrospinning, PVDF/DMF (13 wt%) solutions containing different CNC loadings (0, 1, 3 and 5 % with respect to polymer weight) were first prepared. To this end, CNCs were dispersed in DMF for 15 min under gentle sonication. To make sure that the sonication process did not cause CNC breaking, the WAXD patterns of CNC before (Fig. 5) and after (not shown here) the sonication process were compared, and no significant change was observed. After preparation of CNC/DMF dispersion, a given amount of PVDF powder was dissolved into the sonicated dispersion by magnetic stirring at 60 °C for 24 h. The resultant mixture was subjected to electrospinning under controlled environmental conditions of RH

(relative humidity): 30 % and  $T = 25$  °C. The spinning voltage, working distance and feeding rate of the polymer solution were adjusted to be 15 kV, 15 cm and 1 ml/h, respectively. Electrospun fibers were collected on a grounded rotating collector. Details of the various electrospun PVDF/CNC nanocomposites are listed in Table 1. The procedure to prepare the PVDF/CNC nanocomposite starting from CNC preparation using cotton linters is summarized in a flowchart included in Fig. 1.

#### Scanning electron microscope (SEM)

The electrospun mats as well as CNCs were observed using Zeiss Supra TM 55VP SEM after sputter-coating with gold. The mean diameters of PVDF/CNC electrospun fibers with various CNC contents were obtained through averaging over the measured diameters of 100 randomly selected fibers included in SEM images.

#### Transmission electron microscope (TEM)

Morphologies of CNCs were also observed using TEM. CNC dispersion in water was dropped onto a TEM grid and dried in a vacuum oven prior to imaging using a Gatan Orius SC1000 digital camera on a JEOL 2100 transmission electron microscope (TEM) operating at an accelerating voltage of 200 kV.

#### Fourier transfer infrared (FTIR) spectroscopy

FTIR spectra of PVDF/CNC electrospun nanocomposites were collected by 64 scans between 600 and 2000  $\text{cm}^{-1}$  with a resolution of 4  $\text{cm}^{-1}$  using the Bruker 70. FTIR spectra were normalized using the peak centered at 877  $\text{cm}^{-1}$  as the reference band (Yu and Cebe 2009). This makes it possible to quantitatively evaluate the absorbance bands.

#### Differential scanning calorimetry (DSC)

DSC thermographs of PVDF/CNC electrospun nanocomposites were obtained through heating the samples from 25 to 220 °C with a heating rate of 10 °C/min. This was conducted on a TA Instrument Q200 differential scanning calorimeter.

#### Wide-angle X-ray diffraction (WAXD)

WAXD patterns of the CNCs as well as PVDF/CNC electrospun nanocomposites were obtained using a PANalytical XRD diffractometer in the range of  $2\theta = 5^\circ\text{--}40^\circ$ . All of the WAXD patterns were recorded with Cu-K $\alpha$  radiation ( $\lambda = 1.5418$  Å) generated at 40 kV and 20 mA.

#### Nanocomposite piezoelectric testing

To evaluate the piezoelectric performance of the PVDF/CNC electrospun mat of  $50 \pm 10$   $\mu$  thickness, they were cut into  $2 \times 2$   $\text{cm}^2$  pieces and connected on both sides with metal electrodes. Then, the electrodes were connected to a circuit as schematically shown in Fig. 2. The nanocomposite was mechanically impacted by a small plastic hammer with adjustable frequency and pressure using a custom-built cyclic compression tester. The equipment used to evaluate the piezoelectric performance of the produced nanocomposites is schematically illustrated in Fig. 3. In order to reduce the experimental errors, the measurement was repeated five times for each electrospun web, and the average value was reported. It is worth noting that samples were selected from different parts of the electrospun web.

## Results and discussion

Included in Fig. 4 are SEM and TEM images captured from cellulose nanocrystals (CNCs) prepared based on

**Table 1** Specifications of different electrospun PVDF/CNC nanocomposites

Sample code	PVDF concentration (wt%)	Solvent	CNC loading level (with respect to PVDF weight) (%)
W0	13	DMF	0
W1			1
W3			3
W5			5

**Fig. 1** Procedures to prepare the PVDF/CNC nanocomposite starting from CNC preparation using cotton linters

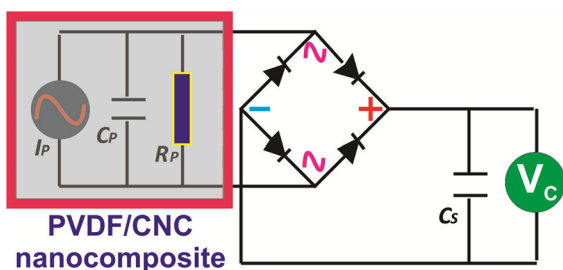
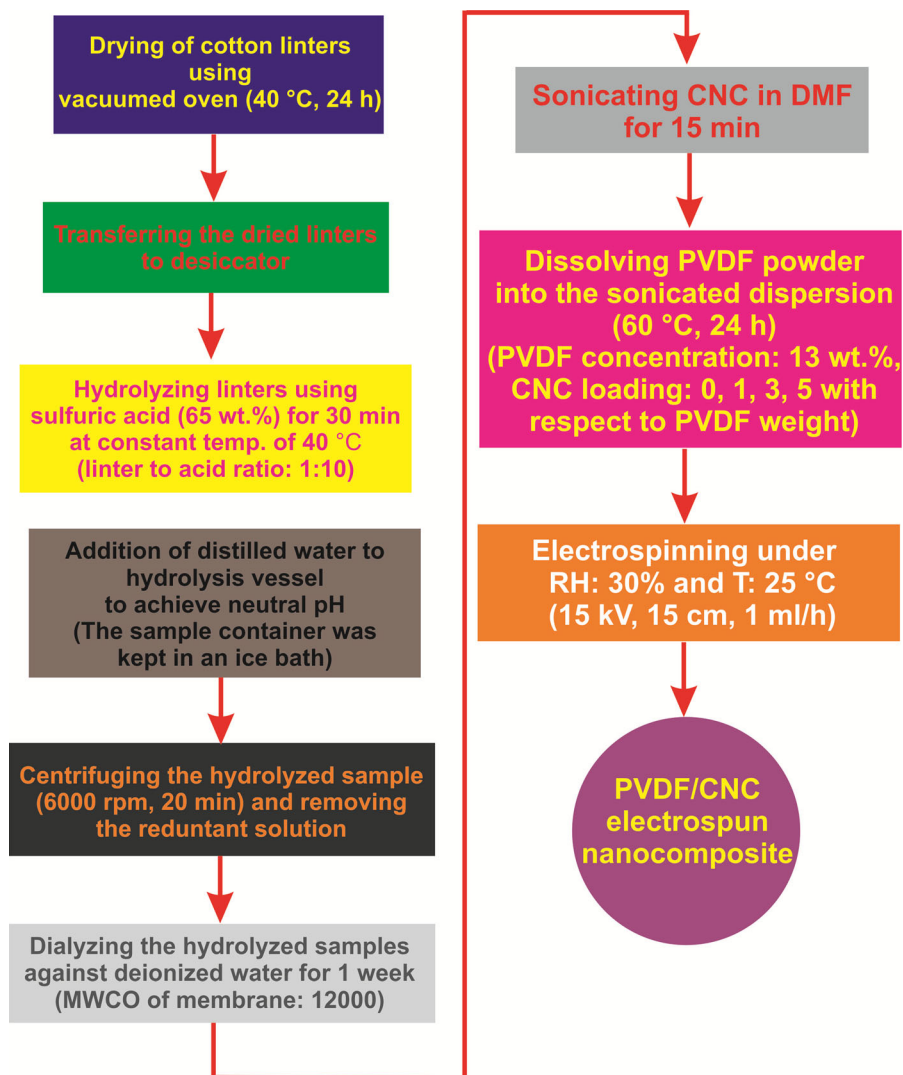


**Fig. 2** Equivalent circuit of charging a capacitor when it was charged by the PVDF/CNC nanocomposite

acid hydrolysis of cotton linters. As can be seen, CNCs are slender whisker-like crystals with lengths of a few hundred nanometers ranging between 50 and 300 nm

and width in the range of 10–20 nm. These dimensions concur well with those measured by Cao et al. (2007).

The WAXD pattern of the CNC sample (Fig. 5) exhibits a high and sharp peak at  $2\theta = 22.7^\circ$  (plane 200) and two weak and overlapping peaks at  $2\theta = 14.9^\circ$  (plane 1–10) and  $2\theta = 16.8^\circ$  (plane 110). Furthermore, a moderate peak can be also observed at  $2\theta = 34^\circ$ , which is a composite of several reflections (French 2014). These crystalline domains feature a typical pattern of cellulose I (French 2014; Jin et al. 2016; French 2013; Henrique et al. 2015). The WAXD pattern of prepared CNCs demonstrates that acid hydrolysis has no disruptive effect on crystalline regions of cotton linters. Strictly speaking, acid hydrolysis using sulfuric acid with a

**Fig. 3** Schematic representation of the piezoelectric test device. A plastic hammer impacted the PVDF/CNC nanocomposite sandwiched between two metal electrodes, and the output voltage was measured by an oscilloscope

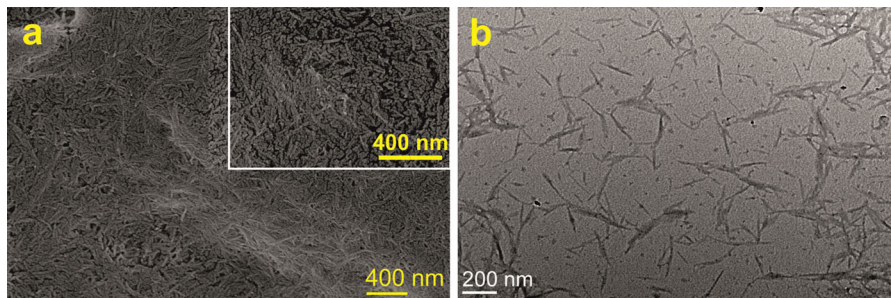
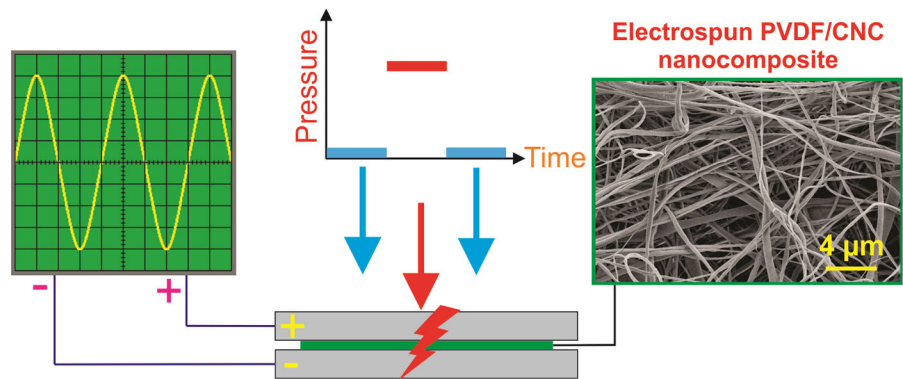


**Fig. 4** **a** SEM and **b** TEM images of CNCs obtained from acid hydrolysis of cotton linters. The *inset* in image **a** is the enlarged view of agglomerated CNCs

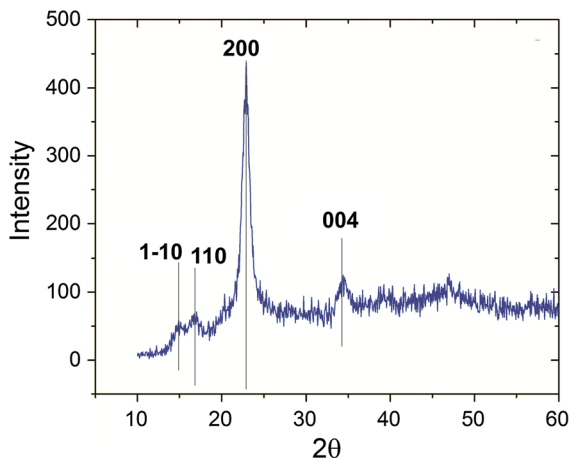


**Fig. 5** WAXD pattern of CNCs obtained from acid hydrolysis of cotton linters

concentration of 65 wt% causes serious damage to the amorphous regions of cotton linters, and the crystalline regions are not attacked.

The prepared CNCs were expected to contribute to the PVDF/CNC electrospun nanocomposites with different polymorphs. SEM images obtained from

the electrospun nanocomposites are illustrated in Fig. 6. As evidenced by this figure, the CNC loading level plays a pivotal role in the morphology of electrospun webs, particularly the fiber diameter. The mean diameters of electrospun fibers with different CNC loadings were measured and are tabulated in Table 2. As shown in Table 2, fibers electrospun from solution with no CNC content, i.e., W0 (see Table 1), have the smallest diameters. Addition of 1 % CNC to the electrospinning solution causes an increase of approximately 63 % in the diameter of electrospun fibers from 439 (W0) to 718 nm (W1). This is while further increasing of the CNC content to amounts higher than 1 %, which leads to thinner fibers. In this regard, three factors could account for the variation of electrospun fiber diameter: surface tension, viscosity and conductivity of the electrospinning solution. The first two parameters resist stretching of the electrospinning jet and lead to thicker fibers. The third parameter favors stretching of the electrospinning jet and is responsible for the formation of thinner fibers.

The variation of PVDF/DMF solution shear viscosity with CNC content is investigated in Fig. 7. As

**Fig. 6** SEM images captured from PVDF/CNC electrospun nanocomposites with different CNC contents with respect to PVDF weight: **a** W0: 0 %, **b** W1: 1 %, **c** W3: 3% and **d** W5: 5 %. The insets show the zoomed-in views of the electrospun mats

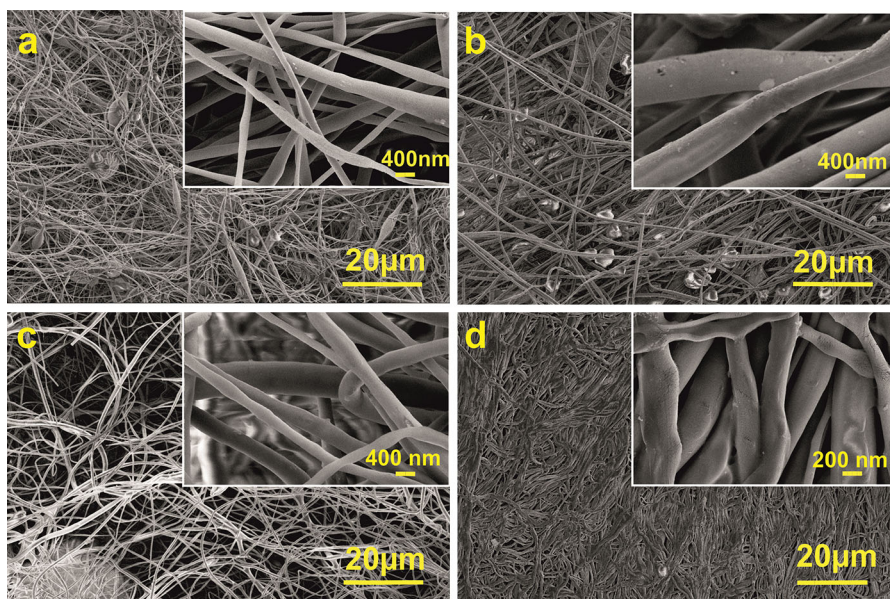


**Table 2** Mean diameters of PVDF/CNC electrospun fibers with different CNC loadings

PVDF/CNC nanocomposite	W0	W1	W3	W5
Mean diameter (SD) (μm)	0.439 (0.152)	0.718 (0.146)	0.552 (0.126)	0.559 (0.135)

SD standard deviation

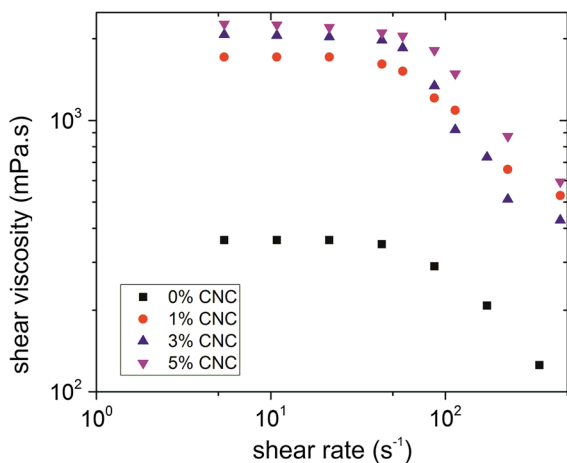


**Fig. 7** Shear viscosity of PVDF/DMF solutions with different CNC contents

depicted, the shear viscosity is directly proportional to the CNC content. The solution with no CNC content has the lowest shear viscosity, while that with 5 % CNC exhibits the highest shear viscosity. The ones with 1 and 3 % CNC loading levels fall between these

two extremes. A similar trend has been also reported by other researchers for PS- and PVDF-based solutions (Zhang et al. 2015; Huan et al. 2015). The variation of electrical conductivity and surface tension of the electrospinning solution with CNC content is investigated in Table 3. As is obvious, there is no significant change in the surface tension of PVDF/DMF solution with increasing CNC content. However, the electrical conductivity of PVDF/DMF solution increases with increasing CNC content. The presence of sulfate groups on the surface of CNC could account for the increased electrical conductivity of the PVDF/DMF/CNC mixture. These groups are produced during hydrolysis by sulfuric acid in order to prepare CNC as fully discussed by Lu and Hsieh (Lu and Hsieh 2010). An increase in the polymer solution conductivity and slight decrease in surface tension as a result of CNC incorporation were also observed by Huan et al. (2015) for PS/(DMF/THF: 3/1) solutions.

Given the above discussion, one may conclude that increasing the electrospun fiber diameter with 1 % CNC loading in comparison to one with 0 % CNC

**Table 3** Electrical conductivity and surface tension of PVDF/DMF solutions with different CNC contents

Sample	W0	W1	W3	W5
Electrical conductivity ( $\mu\text{S}$ )	5.82	20.08	40.70	60.17
Surface tension (mN/m) (SD)	38.06 (0.026)	37.93 (0.151)	37.73 (0.133)	37.91 (0.081)

SD standard deviation

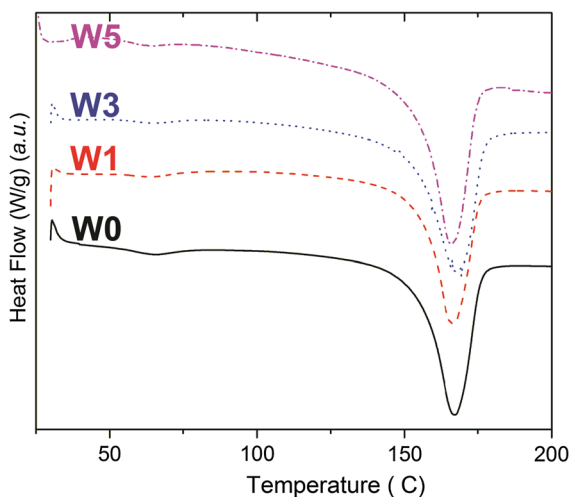
loading can be assigned to the significantly increased shear viscosity of the electrospinning solution. At higher CNC contents, i.e., 3 and 5 %, the slightly increased shear viscosity compared to 1 % CNC loading cannot explain the reduction in fiber diameter. As such, it can be concluded that the significantly increased conductivity of the electrospinning solution dominates the trend observed for the electrospun fiber diameter, and hence thinner fibers with diameters comparable to those of the W0 sample are expected.

The thermal behavior of different electrospun nanocomposites has been investigated in Fig. 8 based on DSC thermographs. As shown, all samples exhibit an endothermic peak around 165 °C denoting the melting of PVDF crystals. The melting enthalpies ( $\Delta H_m$ ) of the nanocomposites with different CNC loadings along with their crystallinity ( $X_c$ ) are listed in Table 4.  $X_c$  was calculated using Eq. 1 in which  $\Delta H_m^*$  and  $\emptyset$  denote the melting enthalpy of a sample with 100 % crystallinity and weight fraction of PVDF in the composite, respectively (Zhang et al. 2015; Ma

et al. 2007). For the PVDF sample,  $\Delta H_m^* = 104.5 \text{ J/g}$  was obtained from Nakagawa and Ishida (1973).

$$X_c(\%) = \frac{\Delta H_m}{\emptyset \cdot \Delta H_m^*} \times 100 \quad (1)$$

Figure 8 and the data included in Table 4 show the significant influence of CNC on the crystallinity characteristics of PVDF/CNC electrospun nanocomposites. In spite of the melting temperature of samples showing no significant dependence on the CNC content, the  $X_c$  parameter measured for various samples is a strong function of the CNC content. CNC loading of 1 % reduces the  $X_c$  in comparison with the sample electrospun from pure PVDF. Further increasing of the CNC loading leads to a nanocomposite with higher crystallinity. Although DSC graphs afford some information about the crystallinity features of the produced nanocomposites, they do not provide a detailed description on the polymorphism variations of nanocomposites as a result of changing the CNC content. To obtain more insight into the polymorphism variations of PVDF/CNC nanocomposites as a function of the CNC loading level, the WAXD patterns (Fig. 9) and FTIR spectra (Fig. 10) were obtained. As shown in Fig. 9, sample W0 has three distinct peaks in its spectrum. These peaks have been centered at  $2\theta = 18.5^\circ$ ,  $19.96^\circ$  and  $27.0^\circ$  corresponding to reflections of the  $\alpha$  (020),  $\beta$  [(200), (110)] and  $\alpha$  (111) PVDF crystalline phases, respectively (Yee et al. 2007; Abolhasani et al. 2014a; Yu and Cebe 2009; Fashandi et al. 2015). Furthermore, it can be clearly seen that addition of 1 % CNC to the electrospinning solution is sufficient to completely remove the  $\alpha$ -related peaks (see the WAXD pattern of W1) and consequently reduced crystallinity of W1, which is in agreement with the DSC results (Fig. 8; Table 4). Further addition of CNC, i.e., 3 and 5 %, results in the intensity of the  $\alpha$  peak at  $2\theta = 18.5^\circ$  being slightly increased compared to that of the sample with 1 % CNC. Besides, for CNC contents

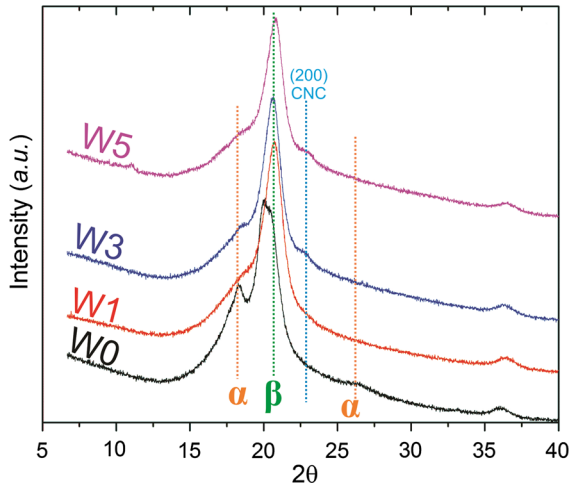
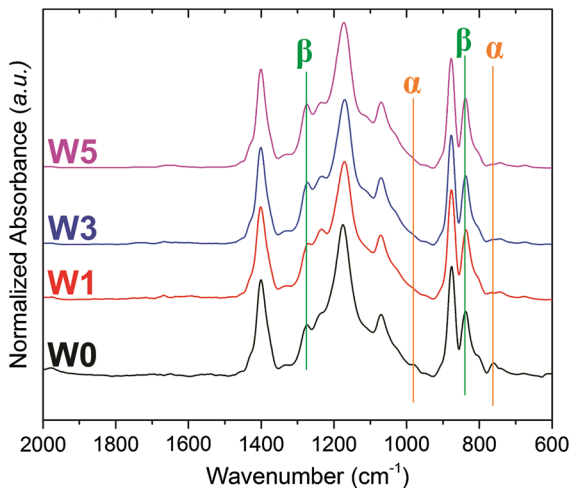


**Fig. 8** DSC thermographs (Exo. up) of PVDF/CNC electrospun nanocomposites with different CNC contents with respect to PVDF weight: W0: 0, W1: 1, W3: 3 and W5: 5 %



**Table 4** Results obtained from DSC thermographs of different PVDF/CNC nanocomposites

PVDF/CNC nanocomposite	W0	W1	W3	W5
Melting temperature (°C)	165.75	165.11	165.88	165.76
Melting enthalpy (J/g)	32.65	28.29	33.68	35.98
$X_c$ (%)	31.24	27.35	33.23	36.24

**Fig. 9** WAXD patterns of PVDF/CNC electrospun nanocomposites with different CNC contents with respect to PVDF weight: W0: 0, W1: 1, W3: 3 and W5: 5 %**Fig. 10** FTIR spectra of PVDF/CNC electrospun nanocomposites with different CNC contents with respect to PVDF weight: W0: 0, W1: 1, W3: 3 and W5: 5 %

over 1 %, the intensity of the  $\beta$  peak is an increasing function of the CNC content. Based on the WAXD patterns, one can conclude that the 1 % CNC loading

is the optimum concentration to completely remove the  $\alpha$  crystalline phases. However, nanocomposites with higher crystallinity and enhanced  $\beta$  crystalline phases are yielded at higher CNC contents, i.e., 3 and 5 %. It is of special note that the shoulders appearing at  $2\theta = 22.7^\circ$  in the WAXD patterns of samples W1, W3 and W5 are associated with the presence of CNC (plane 200) in the electrospun nanocomposites.

To further verify the results of X-ray diffraction experiments, normalized FTIR spectra of different nanocomposites are investigated in Fig. 10. As shown, peaks observed at wavenumbers of 765 and 975  $\text{cm}^{-1}$  are assigned to the  $\alpha$  phase with chain conformations of short trans sequences. Additionally, the peaks appearing at wavenumbers of 840 and 1275  $\text{cm}^{-1}$  correspond to the  $\beta$  phase with long trans sequences (Abolhasani 2015; Abolhasani et al. 2014b, 2015a). This clearly shows that there is very good correlation between the results of the FTIR and X-ray diffraction experiments. Addition of 1 % CNC into the PVDF polymer matrix results in the disappearance of the  $\alpha$ -related peaks (see the FTIR spectrum of W1). Additionally, at higher CNC contents, i.e., 3 and 5 %, higher intensity  $\beta$ -related peaks can be observed (Fig. 10). Based on the results of FTIR and X-ray diffraction experiments, it can be said that at the optimum concentration, CNCs have the ability to nucleate the  $\beta$  phase. It is expected that as a result of this nucleation effect, the piezoelectric performance of PVDF/CNC nanocomposites is improved. This is confirmed by evaluating the piezoelectric output of PVDF/CNC electrospun nanocomposites with a variety of CNC loading levels.

Figure 11 shows the open circuit voltage and short circuit current for the W0 sample. To make sure the signal observed is solely related to the piezoelectric effect, the connection was switched by changing the negative and positive electrodes. As evidenced by Fig. 12, the front peak and back peak positions have been reversed. This observation further demonstrates

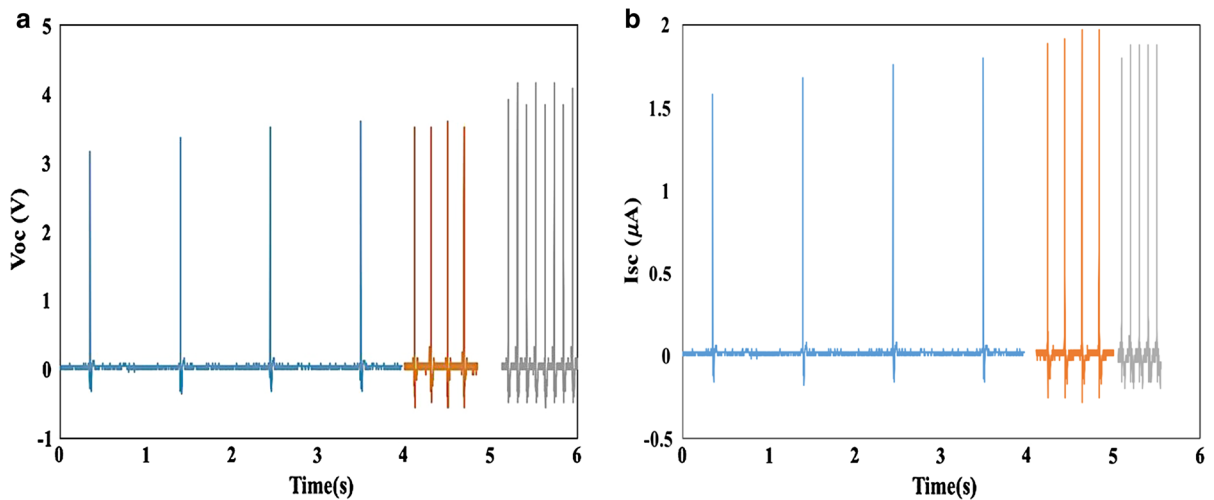


**Fig. 11** a Voc and b Isc values of WO dope

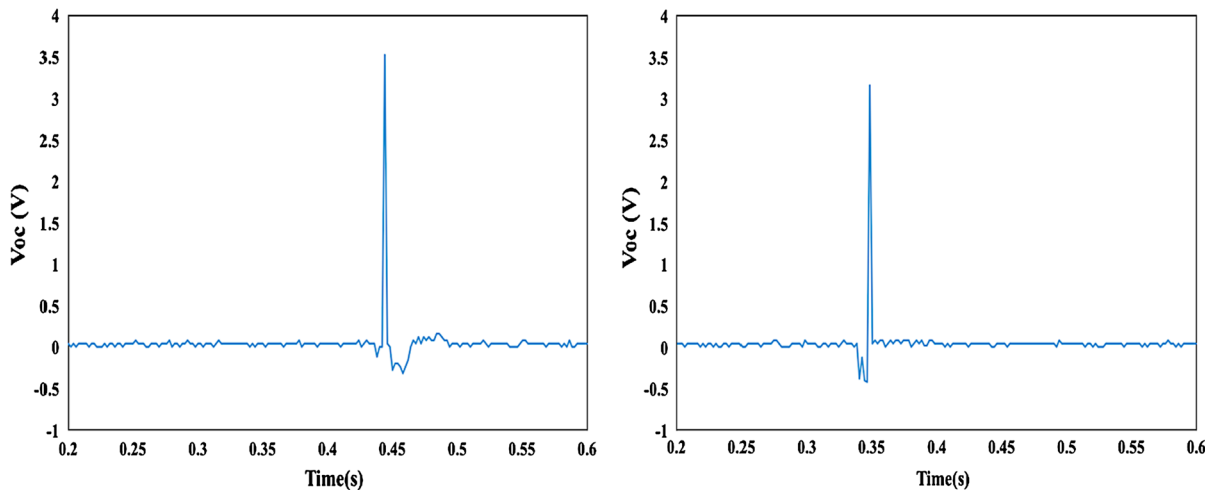


**Fig. 12** Changing the negative and positive electrode has reversed the front and back peak position

that dipoles in the nanofibers have been oriented along the mat thickness as proposed by Mandal (Mandal et al. 2011). Furthermore, Fig. 11 demonstrates that Voc is almost independent of frequency, which helps the regular output to be received from body motions under various frequencies. Table 5 shows the influence of the CNC content on the electrical output of PVDF/CNC generators. It is clear that the output voltage of generators decreased from 3.5 to 2 V with the addition of 1 % CNC to the PVDF nanofibers and then increased to more than 6 V with further addition of CNC. These outputs are completely comparable to the electrical output of the previously developed

**Table 5** Open circuit voltage versus CNC content

CNC content (%)	0	1	3	5
V <sub>oc</sub> (V) (SD)	3.5 (0.2)	2.1 (0.1)	6.2 (0.5)	6.3 (0.6)

SD standard deviation of measurements

PVDF/CNT (8 V) (Liu et al. 2013) and P(VDF-HFP)/silver (3 V) (Mandal et al. 2014) nanofiber generators. These observations can be interpreted by the change in polymorphism of the produced nanocomposite with CNC content. As discussed above, the W1 sample has lower crystallinity and  $\beta$

phase content compared to the other samples (refer to Table 4), which results in its lower electrical outputs. In contrast, the W3 and W5 samples benefit from a higher crystallinity and enhanced  $\beta$  phase, both of which account for more efficient electrical outputs.

Figure 11 demonstrates that, using a simple bridge, the AC output can be transferred into a pulsed rectified output. The electrical output of samples W3 and W5 can easily charge a 33- $\mu$ F capacitor over 6 V, and this voltage is enough to light up a commercial LED for more than 30 s while the capacitor still has the power (Video S1).

From another point of view, one cannot rule out the piezoelectricity of CNC, such that the permanent dipole momentum of CNCs results in the piezoelectric effect of cellulose nanofibril (CNF) film as recently shown by Rajala et al. (2016). Therefore, it may be concluded that CNCs contribute to the measured piezoelectric response of the produced PVDF/CNC nanocomposites. In this regard, it is worth noting that, as evaluated by Rajala et al., the piezoelectric properties of CNCs are lower than those of PVDF-based structures. Furthermore, they used CNFs to make piezoelectric film containing a high level of CNC (maybe 70 %), whereas here the maximum amount of CNC in the produced nanocomposites is 5 % with respect to PVDF weight. Hence, it is far from reality that such a small amount of CNC with a lower piezoelectric response can increase the voltage output of PVDF nanofibers. For example, Shin et al. (2014) used 30 % BaTiO<sub>3</sub> to increase the piezoelectric response of the P(VDF-HFP) composite thin film. Additionally, it is worth mentioning that the electric field generated during electrospinning was <0.1 MV/m, which is 50 times lower than the coercive electric field of CNC. These findings demonstrate the true potential of our PVDF/CNC electrical generator to be used as a self-powering device to charge portable electronic devices.

## Conclusion

PVDF/CNC nanocomposites with various CNC contents, i.e. 0, 1, 3 or 5 %, were electrospun, and their piezoelectric performances were explored for the first time. Analytical techniques such as DSC, FTIR and WAXD were used to study the polymorphism of the produced electrospun nanocomposites. The results

demonstrated the significant influence of CNC on  $\beta$  phase nucleation and enhancing of the  $\beta$  polymorph, which is achieved at the optimum CNC concentration, i.e., 3 and 5 %. It was also observed that  $\alpha$  crystalline phases are not present within the structure of PVDF/CNC nanocomposites. The piezoelectric performance study of the PVDF/CNC nanocomposites revealed that samples with 3 and 5 % of CNC can easily charge a 33- $\mu$ F capacitor over 6 V. The ability of the samples to light up a commercial LED for more than 30 s was also demonstrated. To the best of our knowledge, this is the first time that electrical generators that have potential for development in self-powering devices have been developed based on PVDF/CNC electrospun nanocomposites.

## References

- Abolhasani MM (2015) Effects of dynamic vulcanization on the kinetics of isothermal crystallization in a miscible polymer blend. *New J Chem* 39:6130–6140
- Abolhasani MM, Naebe M, Guo Q (2014a) A new approach for mechanisms of ferroelectric crystalline phase formation in PVDF nanocomposites. *Phys Chem Chem Phys* 16:10679–10687
- Abolhasani MM, Naebe M, Jalali-Arani A, Guo Q (2014b) Crystalline structures and  $\alpha \rightarrow \beta$  and  $\gamma$  polymorphs transformation induced by nanoclay in PVDF-based nanocomposite. *NANO* 9:1450065
- Abolhasani MM, Zarejousheghani F, Cheng Z, Naebe M (2015a) A facile method to enhance ferroelectric properties in PVDF nanocomposites. *RSC Adv* 5:22471–22479
- Abolhasani MM, Ashjari M, Azimi S, Fashandi H (2015b) Investigation of an abnormal  $\alpha$  polymorph formation in miscible PVDF nanocomposite blend using kinetics of crystallization. *Macromol Chem Phys* 217:543–553
- Abolhasani MM, Azimi S, Fashandi H (2015c) Enhanced ferroelectric properties of electrospun poly(vinylidene fluoride) nanofibers by adjusting processing parameters. *RSC Adv* 5:61277–61283
- Abolhasani MM, Fashandi H, Naebe M (2016) Crystalline polymorph transition in poly(vinylidene fluoride)(PVDF)/acrylic rubber (ACM)/clay partially miscible hybrid. *Polym Bull* 73:65–73
- Ahn Y, Lim JY, Hong SM, Lee J, Ha J, Choi HJ et al (2013) Enhanced piezoelectric properties of electrospun poly(vinylidene fluoride)/multiwalled carbon nanotube composites due to high  $\beta$ -phase formation in poly(vinylidene fluoride). *J Phys Chem C* 117:11791–11799
- Baniasadi M, Huang J, Xu Z, Moreno S, Yang X, Chang J et al (2015) High-performance coils and yarns of polymeric piezoelectric nanofibers. *ACS Appl Mater Interfaces* 7:5358–5366
- Baniasadi M, Xu Z, Hong S, Naraghi M, Minary-Jolandan M (2016) Thermo-electromechanical behavior of piezoelectric nanofibers. *ACS Appl Mater Interfaces* 8:2540–2551

- Baqeri M, Abolhasani MM, Mozdianfard MR, Guo Q, Oroumei A, Naebe M (2015) Influence of processing conditions on polymorphic behavior, crystallinity, and morphology of electrospun poly(vinylidene fluoride) nanofibers. *J Appl Polym Sci* 132:1–10
- Cao X, Dong H, Li CM (2007) New nanocomposite materials reinforced with flax cellulose nanocrystals in waterborne polyurethane. *Biomacromolecules* 8:899–904
- Cao Y, Zavatteri P, Youngblood J, Moon R, Weiss J (2015) The influence of cellulose nanocrystal additions on the performance of cement paste. *Cem Concr Compos* 56:73–83
- Cha SN, Seo J-S, Kim SM, Kim HJ, Park YJ, Kim S-W et al (2010) Sound-driven piezoelectric nanowire-based nanogenerators. *Adv Mater* 22:4726–4730
- Cha S, Kim SM, Kim H, Ku J, Sohn JI, Park YJ et al (2011) Porous PVDF as effective sonic wave driven nanogenerators. *Nano Lett* 11:5142–5147
- Chang C, Tran VH, Wang J, Fuh Y-K, Lin L (2010) Direct-write piezoelectric polymeric nanogenerator with high energy conversion efficiency. *Nano Lett* 10:726–731
- Chang J, Dommer M, Chang C, Lin L (2012) Piezoelectric nanofibers for energy scavenging applications. *Nano Energy* 1:356–371
- Chen D, Zhang JXJ (2015) Microporous polyvinylidene fluoride film with dense surface enables efficient piezoelectric conversion. *Appl Phys Lett* 106:193901
- Chen X, Xu S, Yao N, Shi Y (2010) 1.6 V nanogenerator for mechanical energy harvesting using PZT nanofibers. *Nano Lett* 10:2133–2137
- Choi D, Choi M-Y, Choi WM, Shin H-J, Park H-K, Seo J-S et al (2010) Fully rollable transparent nanogenerators based on graphene electrodes. *Adv Mater* 22:2187–2192
- Ding Y, Duan Y, Huang Y (2015) Electrohydrodynamically printed, flexible energy harvester using in situ poled piezoelectric nanofibers. *Energy Technol* 3:351–358
- El Achaby M, Arrakhiz FZ, Vaudreuil S, Essassi EM, Quiss A (2012) Piezoelectric  $\beta$ -polymorph formation and properties enhancement in graphene oxide—PVDF nanocomposite films. *Appl Surf Sci* 258:7668–7677
- Fashandi H, Yegane A, Abolhasani MM (2015) Interplay of liquid-liquid and solid-liquid phase separation mechanisms in porosity and polymorphism evolution within poly(vinylidene fluoride) nanofibers. *Fibers Polym* 16:326–344
- French AD (2013) Idealized powder diffraction patterns for cellulose polymorphs. *Cellulose* 21:885–896
- French AD (2014) Idealized powder diffraction patterns for cellulose polymorphs. *Cellulose* 21:885–896
- Gheibi A, Bagherzadeh R, Merati AA, Latifi M (2014) Electrical power generation from piezoelectric electrospun nanofibers membranes: electrospinning parameters optimization and effect of membranes thickness on output electrical voltage. *J Polym Res* 21:1–14
- Habibi Y, Lucia LA, Rojas OJ (2010) Cellulose nanocrystals: chemistry, self-assembly, and applications. *Chem Rev* 110:3479–3500
- Hadimani RL, Bayramol DV, Sion N, Shah T, Limin Q, Shaoxin S et al (2013) Continuous production of piezoelectric PVDF fibre for e-textile applications. *Smart Mater Struct* 22:075017
- Henrique MA, Flauzino Neto WP, Silvério HA, Martins DF, Gurgel LVA, Barud HdS et al (2015) Kinetic study of the thermal decomposition of cellulose nanocrystals with different polymorphs, cellulose I and II, extracted from different sources and using different types of acids. *Ind Crops Prod* 76:128–140
- Huan S, Bai L, Liu G, Cheng W, Han G (2015) Electrospun nanofibrous composites of polystyrene and cellulose nanocrystals: manufacture and characterization. *RSC Adv* 5:50756–50766
- Jin E, Guo J, Yang F, Zhu Y, Song J, Jin Y et al (2016) On the polymorphic and morphological changes of cellulose nanocrystals (CNC-I) upon mercerization and conversion to CNC-II. *Carbohydr Polym* 143:327–335
- Lalia BS, Samad YA, Hashaikh R (2012) Nanocrystalline cellulose-reinforced composite mats for lithium-ion batteries: electrochemical and thermomechanical performance. *J Solid State Electrochem* 17:575–581
- Lee M, Chen C-Y, Wang S, Cha SN, Park YJ, Kim JM et al (2012) A hybrid piezoelectric structure for wearable nanogenerators. *Adv Mater* 24:1759–1764
- Lee J-H, Lee KY, Kumar B, Tien NT, Lee N-E, Kim S-W (2013) Highly sensitive stretchable transparent piezoelectric nanogenerators. *Energy Environ Sci* 6:169–175
- Lin Y-F, Song J, Ding Y, Lu S-Y, Wang ZL (2008) Alternating the output of a CdS nanowire nanogenerator by a white-light-stimulated optoelectronic effect. *Adv Mater* 20:3127–3130
- Liu Y-L, Li Y, Xu J-T, Fan Z-Q (2010) Cooperative effect of electrospinning and nanoclay on formation of polar crystalline phases in poly(vinylidene fluoride). *ACS Appl Mater Interfaces* 2:1759–1768
- Liu Z, Pan C, Lin L, Lai H (2013) Piezoelectric properties of PVDF/MWCNT nanofiber using near-field electrospinning. *Sens Actuators A* 193:13–24
- Lu P, Hsieh Y-L (2010) Preparation and properties of cellulose nanocrystals: rods, spheres, and network. *Carbohydr Polym* 82:329–336
- Lu M-Y, Song J, Lu M-P, Lee C-Y, Chen L-J, Wang ZL (2009) ZnO–ZnS heterojunction and ZnS nanowire arrays for electricity generation. *ACS Nano* 3:357–362
- Ma W, Zhang J, Wang X, Wang S (2007) Effect of PMMA on crystallization behavior and hydrophilicity of poly(vinylidene fluoride)/poly(methyl methacrylate) blend prepared in semi-dilute solutions. *Appl Surf Sci* 253:8377–8388
- Mandal D, Yoon S, Kim KJ (2011) Origin of piezoelectricity in an electrospun poly(vinylidene fluoride-trifluoroethylene) nanofiber web-based nanogenerator and nano-pressure sensor. *Macromol Rapid Commun* 32:831–837
- Mandal D, Henkel K, Schmeißer D (2014) Improved performance of a polymer nanogenerator based on silver nanoparticles doped electrospun P(VDF–HFP) nanofibers. *Phys Chem Chem Phys* 16:10403–10407
- Mao Y, Zhao P, McConohy G, Yang H, Tong Y, Wang X (2014) Sponge-like piezoelectric polymer films for scalable and integratable nanogenerators and self-powered electronic systems. *Adv Energy Mater* 4:1–7
- Martins P, Lopes AC, Lanceros-Mendez S (2014) Electroactive phases of poly(vinylidene fluoride): determination, processing and applications. *Prog Polym Sci* 39:683–706

- Nakagawa K, Ishida Y (1973) Annealing effects in poly(vinylidene fluoride) as revealed by specific volume measurements, differential scanning calorimetry, and electron microscopy. *J Polym Sci Polym Phys Ed* 11:2153–2171
- Peresin MS, Habibi Y, Zoppe JO, Pawlak JJ, Rojas OJ (2010) Nanofiber composites of polyvinyl alcohol and cellulose nanocrystals: manufacture and characterization. *Biomacromolecules* 11:674–681
- Persano L, Dagdeviren C, Su Y, Zhang Y, Girardo S, Pisignano D et al (2013) High performance piezoelectric devices based on aligned arrays of nanofibers of poly(vinylidene-fluoride-co-trifluoroethylene). *Nat Commun* 4:1633
- Pörhönen J, Rajala S, Lehtimäki S, Tuukkanen S (2014) Flexible piezoelectric energy harvesting circuit with printable supercapacitor and diodes. *IEEE Trans Electron Dev* 61:3303–3308
- Pu J, Yan X, Jiang Y, Chang C, Lin L (2010) Piezoelectric actuation of direct-write electrospun fibers. *Sens Actuators A* 164:131–136
- Pu X, Li L, Song H, Du C, Zhao Z, Jiang C et al (2015) A self-charging power unit by integration of a textile triboelectric nanogenerator and a flexible lithium-ion battery for wearable electronics. *Adv Mater* 27:2472–2478
- Rajala S, Siponkoski T, Sarlin E, Mettänen M, Vuoriluoto M, Pammo A et al (2016) Cellulose nanofibril film as a piezoelectric sensor material. *ACS Appl Mater Interfaces* 8:15607–15614
- Seminara L, Capurro M, Cirillo P, Cannata G, Valle M (2011) Electromechanical characterization of piezoelectric PVDF polymer films for tactile sensors in robotics applications. *Sens Actuators A* 169:49–58
- Shi Q, Zhou C, Yue Y, Guo W, Wu Y, Wu Q (2012) Mechanical properties and in vitro degradation of electrospun bio-nanocomposite mats from PLA and cellulose nanocrystals. *Carbohydr Polym* 90:301–308
- Shin S-H, Kim Y-H, Lee MH, Jung J-Y, Nah J (2014) Hemispherically aggregated BaTiO<sub>3</sub> nanoparticle composite thin film for high-performance flexible piezoelectric nanogenerator. *ACS Nano* 8:2766–2773
- Shiyong X, Yong S, Sang-Gook K (2006) Fabrication and mechanical property of nano piezoelectric fibres. *Nanotechnology* 17:4497
- Soin N, Shah TH, Anand SC, Geng J, Pornwannachai W, Mandal P et al (2014) Novel “3-D spacer” all fibre piezoelectric textiles for energy harvesting applications. *Energy Environ Sci* 7:1670–1679
- Sun LL, Li B, Zhang ZG, Zhong WH (2010) Achieving very high fraction of  $\beta$ -crystal PVDF and PVDF/CNF composites and their effect on AC conductivity and microstructure through a stretching process. *Eur Polym J* 46:2112–2119
- Wang ZL, Song J (2006) Piezoelectric nanogenerators based on zinc oxide nanowire arrays. *Science* 312:242–246
- Wang X, Song J, Zhang F, He C, Hu Z, Wang Z (2010) Electricity generation based on one-dimensional group-III nitride nanomaterials. *Adv Mater* 22:2155–2158
- Xie Y, Wang S, Lin L, Jing Q, Lin Z-H, Niu S et al (2013) Rotary triboelectric nanogenerator based on a hybridized mechanism for harvesting wind energy. *ACS Nano* 7:7119–7125
- Xie Y, Wang S, Niu S, Lin L, Jing Q, Yang J et al (2014) Grating-structured freestanding triboelectric-layer nanogenerator for harvesting mechanical energy at 85% total conversion efficiency. *Adv Mater* 26:6599–6607
- Yee WA, Kotaki M, Liu Y, Lu X (2007) Morphology, polymorphism behavior and molecular orientation of electrospun poly(vinylidene fluoride) fibers. *Polymer* 48:512–521
- Yee WA, Nguyen AC, Lee PS, Kotaki M, Liu Y, Tan BT et al (2008) Stress-induced structural changes in electrospun poly(vinylidene difluoride) nanofibers collected using a modified rotating disk. *Polymer* 49:4196–4203
- Yu L, Cebe P (2009) Crystal polymorphism in electrospun composite nanofibers of poly(vinylidene fluoride) with nanoclay. *Polymer* 50:2133–2141
- Zeng W, Tao X-M, Chen S, Shang S, Chan HLW, Choy SH (2013) Highly durable all-fiber nanogenerator for mechanical energy harvesting. *Energy Environ Sci* 6:2631–2638
- Zhang Z, Wu Q, Song K, Lei T, Wu Y (2015) Poly(vinylidene fluoride)/cellulose nanocrystals composites: rheological, hydrophilicity, thermal and mechanical properties. *Cellulose* 22:2431–2441
- Zhou C, Chu R, Wu R, Wu Q (2011) Electrospun polyethylene oxide/cellulose nanocrystal composite nanofibrous mats with homogeneous and heterogeneous microstructures. *Biomacromolecules* 12:2617–2625
- Zhu G, Su Y, Bai P, Chen J, Jing Q, Yang W et al (2014) Harvesting water wave energy by asymmetric screening of electrostatic charges on a nanostructured hydrophobic thin-film surface. *ACS Nano* 8:6031–6037
- Zimmermann T, Pöhler E, Geiger T (2004) Cellulose fibrils for polymer reinforcement. *Adv Eng Mater* 6:754–761